

# Radially polarized LG<sub>01</sub>-mode Nd:YAG laser with annular pumping

Zhiqiang Fang · Kegui Xia ·  
Yao Yao · Jianlang Li

Received: 8 November 2013 / Accepted: 25 March 2014 / Published online: 10 April 2014  
© Springer-Verlag Berlin Heidelberg 2014

**Abstract** We demonstrated a radially polarized, LG<sub>01</sub>-mode Nd:YAG laser by applying annular-shaped pump light. The annular profile of the pump light was originated from the mode conversion inside a conventional multimode fiber under off-focus coupling condition. This laser gave a maximum output power of 1.2 W at 1,064 nm with a slope efficiency of 28.3 %.

## 1 Introduction

Over the past several years, the lowest-order Laguerre-Gaussian (LG<sub>01</sub>) mode that has ring-shaped intensity profile has been widely investigated both theoretically and experimentally, owing to their potential applications in the fields such as atomic optics [1, 2], optical manipulation of particles [3, 4], lithography [5] and super resolution [6], etc. For example, for the application in the stimulated emission depletion (STED) microscopy, the annular beam depopulates excited state of the dye molecules and results in a resolution of about 20 nm [6].

Until now, the straightforward routes to generate annular beams (e.g., LG<sub>01</sub> mode) are direct illumination of Gaussian beam on axicon [7], few-mode or hollow fiber [8–10], spiral- or axicon-type holograms [11, 12], spatial light modulator [13], etc. Alternatively, for the capability of scaling to high power, such beams can be extracted directly from a laser resonator by deploying various axisymmetric mode discriminators including birefringent

crystal [14–16], conical elements [17–20], subwavelength grating [21, 22] and others inside the cavity.

Another way to excite LG<sub>01</sub> mode, especially in the laser diode (LD) end-pumped solid-state laser, is to reshape top-hat Gaussian intensity distribution of pump light into annular one [23–27]. This transverse shape transformation of pump light renders its efficient spatial match with the annular field distribution of LG<sub>01</sub> mode inside laser crystal and therefore can afford us an efficient excitation of LG<sub>01</sub> mode. As in a typical example given by Kim et al. [23, 24], LG<sub>01</sub>-mode output was obtained in both neodymium- and erbium-doped yttrium aluminum garnet (Nd:YAG and Er:YAG) lasers where a capillary fiber was used to reshape the pump light into annular intensity distribution. Because there was no mode selective component inside the cavity, and thus this scheme was potentially low cost. Further, with the aid of an intracavity lens, the LG<sub>01</sub>-mode output could be radially polarized for the Er:YAG laser, howbeit it was unpolarized for the Nd:YAG laser.

In this paper, we reported an end-pumped, LG<sub>01</sub>-mode solid-state laser. In our scheme, the gain medium was a Nd:YAG crystal incorporated in a simple plano–plano cavity. Further, the pump light from a pumping LD was coupled into a conventional multimode fiber. By applying a slight off-focus alignment, pump light was reshaped into annular intensity distribution through the mode conversion inside this fiber. With such arrangements, an efficient LG<sub>01</sub>-mode output was obtained and also the output was radially polarized. More details are described as follows.

## 2 Experiment setup and formation of annular pumping profile

The schematic diagram of the experimental setup was given in Fig. 1. The Nd:YAG laser crystal had dimensions

Z. Fang · K. Xia · Y. Yao · J. Li (✉)  
Shanghai Institute of Optics and Fine Mechanics,  
China Academy of Sciences, Shanghai 201800, China  
e-mail: apuli@siom.ac.cn

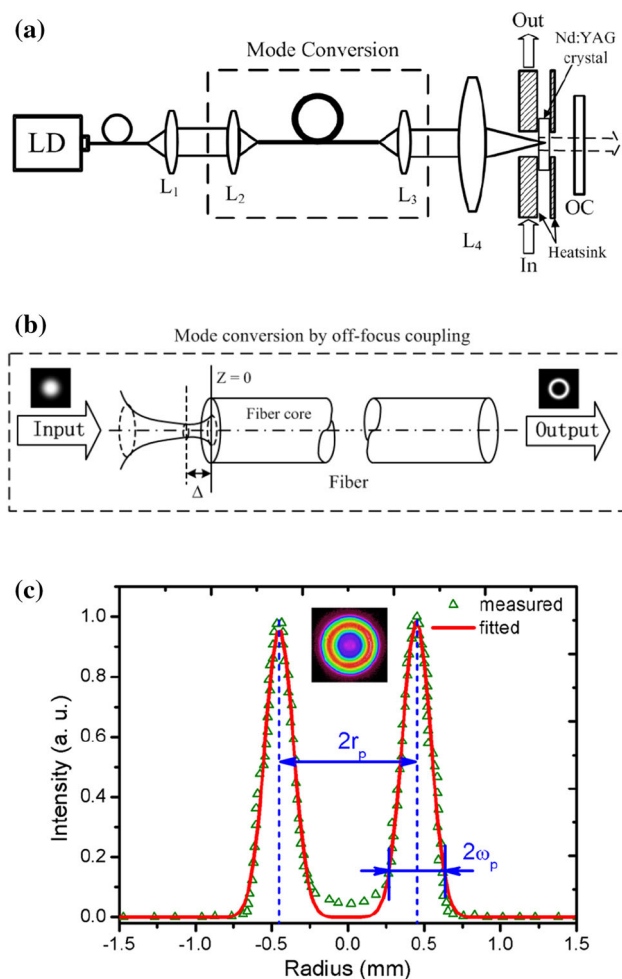


**Fig. 1** **a** Schematic diagram of the end-pumped Nd:YAG laser by using annular pumping. **b** Partial enlarged view of the mode conversion by controlling defocus distance ( $\Delta$ ). **c** Captured intensity distribution of pump light at  $L_4$ 's focal plane by applying 90- $\mu\text{m}$  off-focus coupling and its measured and fitted line intensity profile, in which the parameters of annular pump field  $r_p = 0.44$  mm and  $\omega_p = 183$   $\mu\text{m}$ , respectively

of  $\Phi 10$  mm  $\times$  2 mm and a doping concentration of 1.0 at. % neodymium ions. Its front surface was coated for high transmission at 808 nm and total reflection at 1,064 nm, while its rear surface was antireflection-coated at 1,064 nm. This laser crystal was embedded into two copper plates symmetrically and both the copper plates had 2-mm-diameter light tunnel drilled along the cavity axis. The copper plate clung to the rear surface of Nd:YAG was connected to the 23 °C water cooling. A planar mirror with 2 % transmittance at 1,064 nm was deployed as an output coupler (OC). The total length of laser cavity was 11 cm. The power and intensity profile of laser beam were monitored with a power meter and CCD camera, respectively.

In this setup, a fiber-coupled 808-nm LD was used as the pump source and its pigtail fiber was characterized by a 100- $\mu\text{m}$  core diameter and a 0.22 numerical aperture (NA).

The pump radiation was collimated by an aspherical lens  $L_1$  and focused by an aspherical lens  $L_2$  before being coupled into a conventional step-index MM fiber (400- $\mu\text{m}$  core diameter and NA = 0.37) for the mode conversion. This fiber was 2 m long and was coiled into a circle with a radius of  $\sim 27$  cm without any external strain applied to it. The pump beam exited from this mode conversion fiber then was collimated and focused by lenses  $L_3$  and  $L_4$ , respectively, and thereafter was projected on the central position of front surface of the laser crystal. The focal lengths of  $L_1$ ,  $L_2$ ,  $L_3$  and  $L_4$  were 11, 8, 8 and 25.4 mm, respectively. The NAs of  $L_1$  and  $L_2$  were 0.25 and 0.5, respectively.

Reshaping the pump beam profile into annular shape was realized by adjusting the distance between the focal point of the lens  $L_2$  and the front end face of the mode conversion fiber. Such off-focus alignment was intended for controllable spatial match of launched mode field of pump light with higher-order fiber modes except for the fundamental mode. The following tests were conducted to verify the validity of proposed scheme. When the defocus distance ( $\Delta$  as shown in Fig. 1b) was equal to zero, nearly 100 % pump power was coupled into the conversion fiber and the intensity profile of the pump light at rear end of the fiber kept unchanged with 100 % power transmission efficiency. At 20- $\mu\text{m}$  defocus distance,  $\sim 92$  % power of pump light was coupled into the conversion fiber and the pumping profile behind this fiber kept unchanged with nearly 99 % power transmission efficiency. Nevertheless, when the defocus distance was increased further and reached 90  $\mu\text{m}$ , about 89 % pump power was coupled into the conversion fiber. The pump beam behind the fiber exhibited an annular intensity distribution as depicted in the inset of Fig. 1c, which showed a measured  $M^2$  factor of  $\sim 380$  and about 75 % mode-field conversion efficiency. Further Fig. 1c depicted the line intensity profile of annular pump light at the focal plane of  $L_4$ , in which two parameters  $r_p$  and  $\omega_p$  were defined as the half distance between the two axisymmetric intensity peaks and the half width of  $1/e^2$  peak intensity, respectively.

According to this test described above, although the off-focus coupling of pump light into a MM optical fiber resulted in a slight reduction in the coupling efficiency, the subsequent mode-field conversion inside the fiber rendered that it was an efficient method to transform the top-hat intensity distribution of pump light into annular one.

### 3 Results and discussions

After the annular intensity distribution of pump light was projected into laser crystal, it was observed that the excited laser mode had doughnut-shaped intensity distribution at

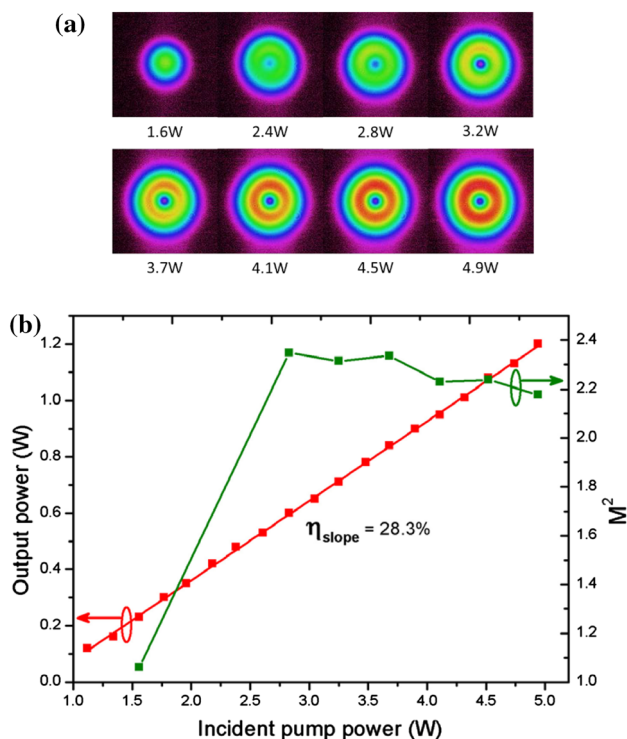


**Fig. 2** **a** Full profiles of laser beam in far-field at different pump powers that incident on laser crystal. **b** Output power and measured beam propagation factor ( $M^2$ ) as function of incident pump power

the pump power higher than the lasing threshold. For definite description, Fig. 2a plots the captured far-field intensity distribution of laser beam at different pump powers where their doughnut shapes can be clearly discerned, although the laser mode seems to be TEM<sub>00</sub>-like mode at lower pump power near the lasing threshold (0.6-W pump power). The TEM<sub>00</sub>-like mode profile of laser beam at lower pump power also was confirmed by the measured beam propagation factor ( $M^2$ ). Figure 2b depicts the measured  $M^2$  factor as a function of incident pump power at 11 cm cavity length. As seen, the measured  $M^2$  factor of laser beam was around 1.1 at low pump power (in the range of 0.6–2.0 W), and then slowly decreased from  $\sim 2.4$  to  $\sim 2.2$  at high pump power. As known, the theoretical  $M^2$  factor is unity for an ideal fundamental Gaussian beam (TEM<sub>00</sub> mode), and it is 2 for an ideal LG<sub>01</sub> mode. Hence, the results in Fig. 2a, b were in good agreement with each other and confirmed that the laser oscillated in TEM<sub>00</sub> mode at the low pump power and doughnut-shaped high-order mode at high pump power. The phenomenon of lasing mode transition with the increase of pump power was attributed to the variation of cavity configuration with thermal lensing effect [28, 29]. At lower pump power near the lasing threshold, the TEM<sub>00</sub> mode had higher spatial match with the annular pumping than that of other lasing modes. When the pump power increased, the thermal

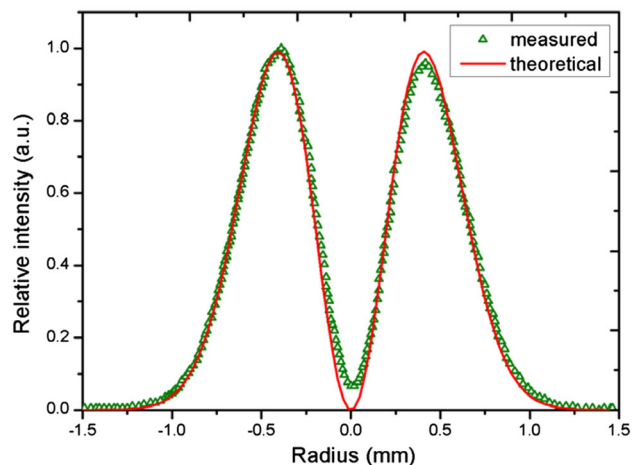


**Fig. 3** The measured and fitted intensity distribution of the doughnut-shaped laser modes at 4.9-W pump power

lensing effect adjusted the cavity configuration. The spatial match between the doughnut-shaped mode and annular pump field surpassed the spatial match between the TEM<sub>00</sub> mode and annular pump field, and thus the doughnut-shaped mode would prefer to oscillate. An optimization of the parameters ( $r_p$  and  $\omega_p$ ) of annular pump field would alleviate TEM<sub>00</sub> oscillation at low pump power.

Figure 2b also shows the variation of laser beam power with incident pump power. As given, the beam power increased linearly with incident pump power with a slope efficiency of 28.3%. At 4.9-W pump power, a maximum beam power of 1.2 W was obtained. In the present arrangement, there was no evidence of thermally-induced roll-over or sudden change [30] in output power, therefore there existed the space to boost the output power once more pump power available.

The doughnut-shaped laser mode obtained at high pump power was further analyzed. Figure 3 plots the measured transverse far-field intensity profile of laser beam along its radial direction at a distance of  $\sim 60$  cm behind the OC and the beam radius is 0.58 mm, in which the beam's doughnut intensity distribution with a central null intensity can be observed. This curve also was fitted theoretically by using a first-order Laguerre-Gaussian function. The good agreement between the theoretical and experimental data on laser beam's intensity distribution verified the laser's oscillation in a pure LG<sub>01</sub> mode.

The polarization states of the doughnut-shaped laser modes were checked by applying a linear polarizer analyzer. For an example, Fig. 4a, b depicts the far- and near-field full beam profiles at 3.2-W pump power, while the images in Fig. 4c–f plot the corresponding far-field intensity distribution of laser beam transmitted through the linear polarizer analyzer. As seen in the pictures, the

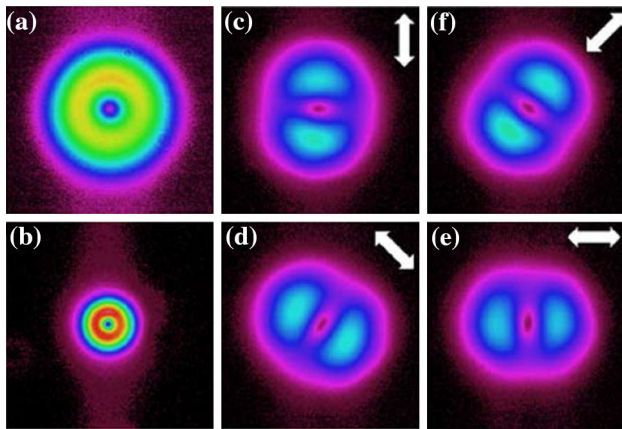


**Fig. 4** **a** Far and **b** near-field intensity distribution of the full beam profile at 3.2-W pump power; **c–f** Intensity profiles of far-field laser beam transmitted through the polarizer analyzer. The *white arrows* indicate the respective orientations of the polarizer analyzer's axis

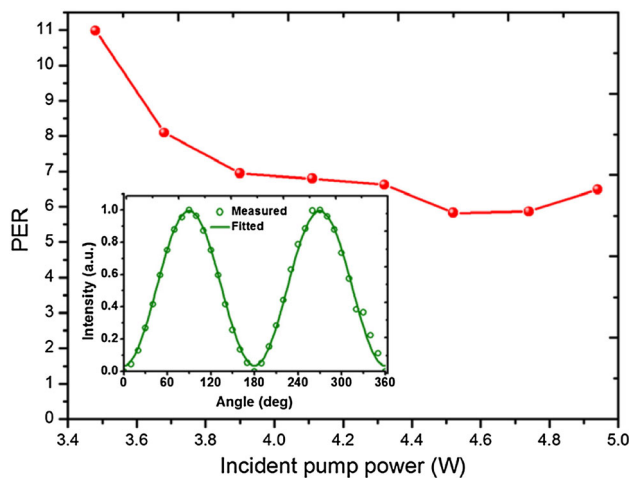


**Fig. 5** Measured PER of radially polarized laser output as a function of incident pump power. *Inset* Transmitted intensity of laser beam through a pinhole aperture when the polarizer analyzer was rotated at different angles at 3.2-W pump power

symmetric two-lobe patterns were always parallel to the respective polarizer axis, and this phenomenon manifested that the doughnut-shaped laser beam was radially polarized.

For an ideal radially polarized beam, at an arbitrary point of the ring profile, the light is locally linearly polarized along its radial direction; therefore, the polarization extinction ratio (PER) of whole vector beam can be represented by the PER of this localized point. Based on this principle, a 0.2-mm-diameter pinhole was placed into the optical path at a distance of 2.1 m behind the OC where the size of the full profile of laser beam was much larger

than this tiny aperture. Adjusting the lateral position of the tiny aperture enabled the transmitted light intensity through it to be maximized. The transmitted light thus was linearly polarized beam and the PER could be measured by using a polarizer analyzer. The inset in Fig. 5 depicts the power variation of the transmitted light through the tiny aperture when rotating the polarizer analyzer at 3.2-W pump power, which implies a PER of 11:1. This PER value corresponded to 83.3 % degree of polarization [31]. The PER of obtained LG<sub>01</sub> mode at different pump powers was also measured in the same way. As illustrated in Fig. 5, it degraded with the increase in pump power.

In our laser resonator, there was not any intracavity polarization-selective component. The physical mechanism responsible for radially polarized excitation in this simple plano–plano laser cavity was attributed to the thermally-induced bifocusing [30, 32–36]. More detailed theoretical explanation for the mechanism is given in the following section.

As we know, temperature gradient in a rod-shaped laser crystal due to an inhomogeneous pumping (heating) produces thermal strain and a transverse gradient of refractive indices. For a paraxial coherent beam propagating in the heated laser crystal, optical path difference (OPD) is derived as [37, 38].

$$\text{OPD} = 2 \int_0^L \left[ \frac{dn}{dT} \Delta T(r, z) + n_0 \varepsilon_{zz} + \sum_{i,j=1}^3 \frac{\partial n}{\partial \varepsilon_{ij}} \varepsilon_{ij} \right] dz \quad (1)$$

where the first term results from the thermal dispersion  $dn/dT$  and temperature difference  $\Delta T(r, z)$ , the second term is caused by the axial strain distribution  $\varepsilon_{zz}$ , and the third term represents the strain induced birefringence with the strain tensor  $\varepsilon_{ij}$ . In the formula,  $r$  represents the radial direction of crystal and the integral is calculated along the cavity axis. In the calculations, we used  $dn/dT = 7.3 \times 10^{-6} \text{ K}^{-1}$  and  $n = 1.82$  for Nd:YAG crystal [38]. Figure 6a plots a typical and numerical result of OPD in Nd:YAG laser crystal where the pump light had 4-W power and annular intensity profile as given in Fig. 1c. As seen, the radially polarized component of LG<sub>01</sub> mode had a larger OPD than azimuthally polarized component. Further, for both components their respective OPD was equated with a pump-dependent thin lens with focal length  $f_i = r^2/\text{OPD}$  [39]. Figure 6b plots the focal lengths of thermal lenses for both radially and azimuthally polarized modes as well as the corresponding stability conditions as a function of incident pump power, respectively. As seen, with the increase of pump power, the thermal lensing effect became much more serious. While the cavity kept stable for both radially and azimuthally polarized components even at 8-W pump power which is higher than the maximum pump power available. Insertion of such thin lens into laser cavity



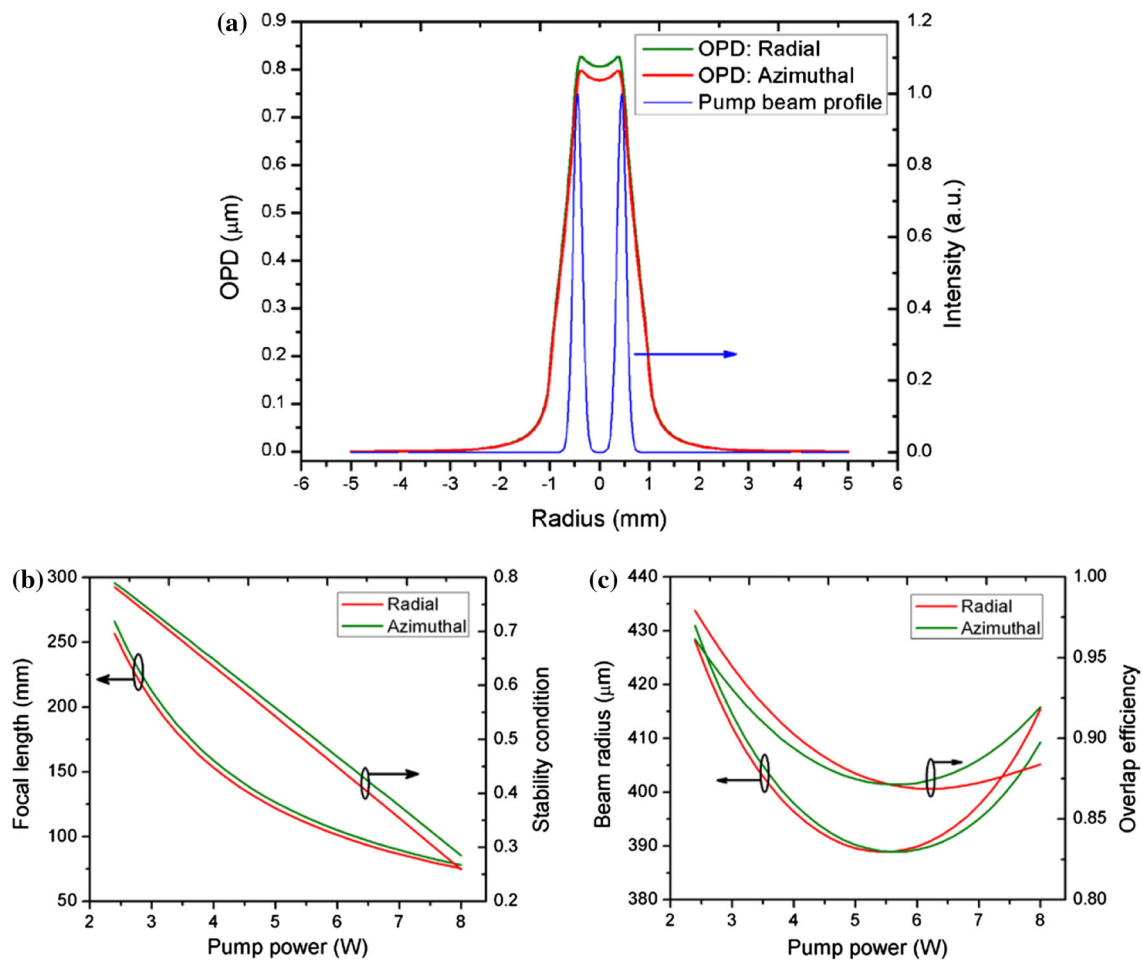


**Fig. 6** **a** Radial distribution of thermal-induced OPDs of radially and azimuthally polarized components under annular pump profile. **b** Thermal focal lengths of both radially and azimuthally polarized components as well as their stability conditions as the functions of

incident pump power, respectively. **c** Transverse sizes of both radially and azimuthally polarized mode components at the front surface of laser crystal as well as their overlap efficiencies with annular pump profile as the functions of incident pump power

caused the difference in transverse mode sizes of these two components, and further induced the difference in overlap efficiencies of these two mode components with the annular pump field.

Figure 6c plots the transverse sizes of both the radially and azimuthally polarized components as well as their overlap efficiencies with annular pumping profile in the front surface of laser crystal as the functions of annular pump power. It was clearly shown that, by applying annular pumping, the transverse size of radially polarized component was smaller than azimuthally polarized component at the pump power lower than 5.5 W, and this resulted in a larger overlap efficiency of former mode component with the annular pumping profile than that of latter mode component. This difference in the overlap efficiencies for them brought a low lasing threshold and high lasing efficiency for radially polarized components, and thus our laser resonator was preferential to oscillate in

this mode. Nevertheless, when the pump power exceeded 5.5 W, the difference in both beam radii of these two mode components as well as their respective spatial overlap efficiencies with annular pump field were reversed. This suggests that the radially polarized laser oscillation would possibly switch to azimuthally polarized at some higher pump power.

#### 4 Conclusions

In summary, we demonstrated a  $LG_{01}$ -mode Nd:YAG laser by applying annular pump light. The annular pumping profile was formed in a conventional multimode fiber through the mode conversion under off-focus coupling condition. The experimental results showed such annular pumping was an efficient method to generate  $LG_{01}$ -mode excitation in an end-pumped solid-state laser resonator.

Further optimization to the length of laser crystal and spatial profile of pump beam can result in significant increases in LG<sub>01</sub>-mode power and laser efficiency, and a proper control to the thermal lens in the laser crystal would build up a thermal-induced polarization filter to force radially polarized oscillation.

## References

1. T. Kuga, Y. Torii, N. Shiokawa, T. Hirano, Y. Shimizu, H. Sasada, *Phys. Rev. Lett.* **78**, 4713 (1997)
2. Y.J. Cai, X.H. Lu, Q. Lin, *Opt. Lett.* **28**, 1084 (2003)
3. H. Kawauchi, K. Yonezawa, Y. Kozawa, S. Sato, *Opt. Lett.* **32**, 1839 (2007)
4. D.G. Grier, *Nature* **424**, 810 (2003)
5. V. Sizyuk, A. Hassanein, T. Sizyuk, *Laser Part. Beams* **25**, 143 (2007)
6. T. Züchner, A.V. Failla, A.J. Meixner, *Angew. Chem. Int. Ed.* **50**, 5274 (2011)
7. J. Arlt, K. Dholakia, *Opt. Commun.* **177**, 297 (2000)
8. J. Yin, H. Noh, K. Lee, K. Kim, Y. Wang, W. Jhe, *Opt. Commun.* **138**, 287 (1997)
9. S. Ramachandran, P. Kristensen, M.F. Yan, *Opt. Lett.* **34**, 2525 (2009)
10. T. Grosjean, M. Suarez, A. Sabac, *Appl. Phys. Lett.* **93**, 231106 (2008)
11. N.R. Heckenberg, R. McDuff, C.P. Smith, A.G. White, *Opt. Lett.* **17**, 221 (1992)
12. C. Paterson, R. Smith, *Opt. Commun.* **124**, 121 (1996)
13. A. Shevchenko, S.C. Buchter, N.V. Tabiryan, M. Kaivola, *Opt. Commun.* **232**, 77 (2004)
14. D. Pohl, *Appl. Phys. Lett.* **20**, 266 (1972)
15. R.J. Zhou, B.I. Escamilla, J.W. Haus, P.E. Powers, Q. Zhan, *Appl. Phys. Lett.* **95**, 191111 (2009)
16. K. Yonezawa, Y. Kozawa, S. Sato, *Opt. Lett.* **31**, 2151 (2006)
17. Y. Kozawa, S. Sato, *Opt. Lett.* **30**, 3063 (2005)
18. J.L. Li, K. Ueda, M. Musha, A. Shirakawa, Z.M. Zhang, *Opt. Lett.* **32**, 1360 (2007)
19. J.F. Bisson, J.L. Li, K. Ueda, Yu. Senatsky, *Opt. Express* **14**, 3304 (2006)
20. K.C. Chang, T. Lin, M.D. Wei, *Opt. Express* **21**, 16035 (2013)
21. J.L. Li, K. Ueda, L.X. Zhong, M. Musha, A. Shirakawa, T. Sato, *Opt. Express* **16**, 10841 (2008)
22. K.G. Xia, K.I. Ueda, J.L. Li, *Appl. Phys. B* **107**, 47 (2012)
23. J.W. Kim, J.I. Mackenzie, J.R. Hayes, W.A. Clarkson, *Opt. Express* **19**, 14526 (2011)
24. J.W. Kim, W.A. Clarkson, *Opt. Commun.* **296**, 109 (2013)
25. Y.F. Chen, Y.P. Lan, S.C. Wang, *Appl. Phys. B* **72**, 167 (2001)
26. Y.F. Chen, Y.P. Lan, *J. Opt. B: Quantum Semiclassical Opt.* **3**, 146 (2001)
27. J.F. Bisson, Yu. Senatsky, K. Ueda, *Laser Phys. Lett.* **2**, 327 (2005)
28. N. Hodgson, H. Weber, *Laser Resonator and Beam Propagation*, 2nd edn. (Springer, Heidelberg, 2005)
29. N. Barre, M. Romanelli, M. Brunel, *Opt. Lett.* **39**, 1022 (2014)
30. A. Ito, Y. Kozawa, S. Sato, *J. Opt. Soc. Am. B* **26**, 708 (2009)
31. A.V. Nesterov, V.G. Niziev, V.P. Yakunin, *J. Phys. D* **32**, 2871 (1999)
32. M.D. Wei, Y.S. Lai, K.C. Chang, *Opt. Lett.* **38**, 2443 (2013)
33. I. Moshe, S. Jackel, A. Meir, *Opt. Lett.* **28**, 807 (2003)
34. G. Machavariani, Y. Lumer, I. Moshe, A. Meir, S. Jackel, N. Davidson, *Appl. Opt.* **46**, 3304 (2007)
35. F. Enderli, T. Feurer, *Opt. Lett.* **34**, 2030 (2009)
36. J.H. Huang, J. Deng, Y.G. Cao, W. Weng, H. Zheng, J.H. Li, F. Shi, Y. Ge, S.T. Dai, W.X. Lin, *Opt. Express* **19**, 2120 (2011)
37. Y.F. Chen, T.M. Huang, C.F. Kao, C.L. Wang, S.C. Wang, *IEEE J. Quantum Electron.* **33**, 1424 (1997)
38. C. Pfistner, R. Weber, H.P. Weber, S. Merazzi, R. Gruber, *IEEE J. Quantum Electron.* **30**, 1605 (1994)
39. X.Y. Peng, L. Xu, A. Asundi, *Opt. Eng.* **43**, 2454 (2004)